Research Square

Preprints are preliminary reports that have not undergone peer review.
They should not be considered conclusive, used to inform clinical practice,
or referenced by the media as validated information.

Microfluidically Reconfigurable Self-Diplexing Half-Mode Substrate Integrated Waveguide MIMO Antenna

KRISHNA REDDY GURRALA
SRM University, Andhra Pradesh
GOUTAM RANA
goutam.r@srmap.edu.in

SRM University, Andhra Pradesh
JYOTIBHUSAN PADHI
SRM University, Andhra Pradesh

Article

Keywords: Deionized water, Microfluidic, Multi-input multi-output, Substrate-integrated waveguide, Self-diplexing

Posted Date: November 16th, 2026

DOI: https://doi.org/10.21203/rs.3.rs-11480591/v1

License: This work is licensed under a Creative Commons Attribution 4.0 International License.
Read Full License

Additional Declarations: No competing interests reported.

Microfluidically Reconfigurable Self-Diplexing Half-Mode Substrate Integrated Waveguide MIMO Antenna

Gurrala Krishna Reddy[1], Goutam Rana[1*], Jyotibhusan Padhi[1*]

[1]Department of Electronics and Communication Engineering, SRM University-AP, Amaravathi, 522240, Andhra Pradesh, India.

*Corresponding author(s). E-mail(s): goutam.r@srmap.edu.in; jyotibhusan.p@srmap.edu.in;
Contributing authors: krishnareddy_gurrala@srmap.edu.in;

Abstract

This paper presents a microfluidically reconfigurable Substrate-Integrated Waveguide (SIW)-based self-diplexing Multiple-Input Multiple-Output (MIMO) antenna for Wi-Fi 6/6E applications. A diagonally shielded Half-Mode SIW (HMSIW) cavity is employed to suppress electromagnetic leakage through the open magnetic wall. A rectangular slot separates the HMSIW cavity into two unequal resonant sections, enabling self-diplexing operation. The two cavities resonate at 5.45 GHz and 6.75 GHz, providing port isolation levels of **40** dB and **35** dB and realized gains of 5.60 dB and 5.65 dB, respectively. Frequency reconfiguration is achieved by incorporating liquid-dielectric pockets on the bottom surface of the cavities, with deionized (DI) water employed as the tuning medium. Adjusting the number of pockets filled with deionized (DI) water enables independent tuning of the lower and upper resonant frequencies across 5.08–5.45 GHz and 6.37–6.75 GHz, respectively. Throughout these tuning ranges, the antenna maintains a realized gain of 5.45–5.65 dB with overall efficiency exceeding 90%. Furthermore, a four-element, eight-port MIMO configuration is developed, achieving an inter-element isolation exceeding 22 dB. The calculated MIMO performance metrics remain within acceptable limits, confirming the suitability of the proposed configuration for MIMO operation. The proposed antenna is fabricated and experimentally evaluated, and the measured results closely agree with the simulated performance.

Keywords: Deionized water, Microfluidic, Multi-input multi-output, Substrate-integrated waveguide, Self-diplexing

1 Introduction

The rapid development of wireless communication technologies has driven the need for compact antennas capable of multi-band operation and frequency reconfiguration. Conventional multi-band antennas[1–5] can support multiple frequency bands

simultaneously through a single feeding port. However, selective operation at an individual frequency band requires an additional high-isolation multiplexer. This increases antenna size, complexity, and adds challenges to system integration.

Therefore, there is a growing need for multi-band antennas with self-multiplexing capability. Several self-diplexing antennas based on microstrip technology have been reported using multi-layer structures [6] and non-planar configurations [7, 8]; however, these antennas face challenges in planar integration. To address this limitation, SIW-based self-diplexing antennas have attracted considerable attention because of their planar structure, cost-effectiveness, and ease of integration. Various SIW-based self-diplexing antennas employing a transfer slot [9], rectangular slot [10], U-shaped slot [11], and bowtie-shaped slot [12] have been reported. However, these designs use full SIW cavities, increasing antenna size. To miniaturize the antenna, researchers have investigated various modes, such as half-mode (HM) [13, 14], quarter-mode (QM) [15–17], and eighth-mode (EM) [18], while maintaining comparable performance. Nevertheless, their open-ended magnetic walls leak RF energy into the substrate, causing unwanted coupling [19].

These antennas are limited to a certain frequency band, which limits their application. Researchers have achieved frequency reconfiguration using PIN/varactor diodes [20–22], MEMS switches [23–25], ferrite substrates [26], and tunable electromagnetic bandgap substrates [27]. However, these approaches generally require biasing networks, which increase system complexity, power consumption, and nonlinear effects.

Recently, microfluidic techniques have emerged as an attractive alternative for realizing bias-free frequency-reconfigurable antennas [28–31]. DI-water-filled polypropylene tubes have been used to demonstrate frequency tuning [28]. M. G. Reddy *et al.* presented a self-diplexing antenna that uses different liquid dielectrics, such as olive oil, transformer oil, acetone, and DI water, for frequency tuning [29]. Similarly, [30] achieves fine-tuning by inserting solid or liquid dielectrics into etched pockets. In [31], an A-shaped slot realizes a frequency-tunable self-diplexing antenna.

The antennas reported in [9–18] exhibit RF leakage through their open magnetic walls, resulting in undesired electromagnetic coupling. In contrast, the tunable antennas reported in [20–27] employ active switching devices, which increase hardware complexity because they require biasing circuits and consume continuous power. Moreover, the frequency-reconfigurable self-diplexing antennas reported in [28–31] are limited to a single radiating element and provide isolation below 30 dB. Multi-input multi-output (MIMO) technology offers significant advantages, including improved communication reliability, increased channel capacity, and enhanced spectral efficiency [32]. However, integrating self-diplexing, microfluidic reconfiguration, and MIMO functionality into a compact SIW antenna has received limited attention. Therefore, developing a compact planar antenna that integrates these functionalities while mitigating electromagnetic leakage and enhancing port isolation is highly desirable.

This paper presents a microfluidically frequency-reconfigurable self-diplexing MIMO antenna based on half-mode SIW technology for Wi-Fi 6/6E applications in the 5- and 6-GHz bands [32, 33]. The open magnetic wall of the half-cavity is shielded to prevent RF energy leakage, while a rectangular slot forms two unequal cavities operating at 5.45 GHz and 6.75 GHz, with isolation exceeding 35 dB. The two resonant frequencies of the self-diplexing antenna are independently tuned using DI-water-loaded pockets located at the bottom of the SIW cavities. We designed a four-element MIMO antenna system that achieves more than 22 dB inter-element isolation. A prototype of the proposed antenna was fabricated and experimentally tested, showing good agreement between simulation and measurement.

2 SELF-DIPLEXING ANTENNA DESIGN

Fig. 1 illustrates the configuration of the proposed microfluidic self-diplexing antenna, realized on a Rogers RT/duroid 5880 substrate with $\varepsilon_r = 2.2$ and $\tan\delta = 0.002$. The successive stages of the antenna development and structural modifications are depicted in Fig. 2.

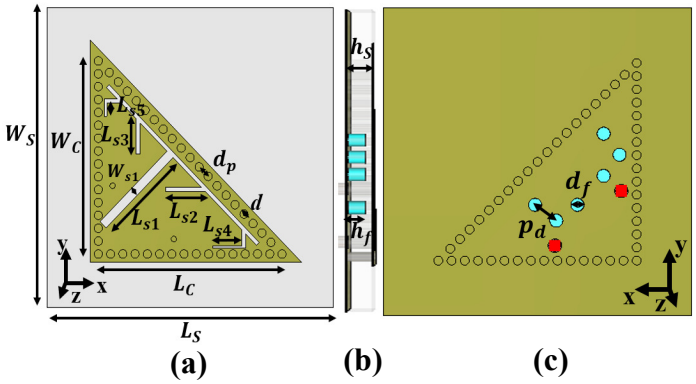


Fig. 1 Microfluidically reconfigurable self-diplexing antenna: (a) top view (b) side view and (c) bottom view. The dimensions are $L_s = W_s = 35$, $L_c = W_c = 25.9$, $L_{s1} = 11.6$, $W_{s1} = 1$, $L_{s2} = 4.87$, $L_{s3} = 4.1$, $L_{s4} = 3.5$, $L_{s5} = 1.5$, $d_p = 1.5$, $d = 1$, $d_f = 1.5$, and $p_d = 2$ (All dimensions are expressed in millimeters(mm)).

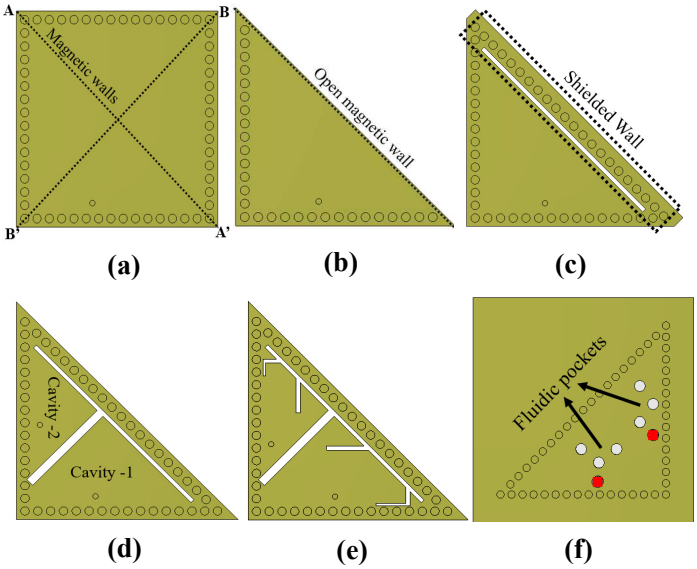


Fig. 2 Development stages of the proposed antenna: (a) full-mode SIW (FMSIW), (b) half-mode SIW (HMSIW), (c) HMSIW with a shielded magnetic wall, (d) Antenna I, (e) Antenna II, and (f) bottom view of Antenna II.

As the initial configuration, we consider a FMSIW square cavity, as illustrated in Fig. 2(a). Its fundamental resonance occurs at 6.57 GHz, corresponding to the TE_{110} mode, as verified by the E-field distribution in Fig. 3(a). The corresponding cavity resonance frequency is calculated from (1).

$$f_{\mathrm{TE}_{110}(\mathrm{FM})} = \frac{c}{2\sqrt{\varepsilon_r}}\sqrt{\left(\frac{1}{W_{\mathrm{eff}}}\right)^2 + \left(\frac{1}{L_{\mathrm{eff}}}\right)^2} \quad ----------(1)$$

$$W_{\text{eff}} = L_C - \frac{d^2}{0.95p_d}$$

$$L_{\text{eff}} = W_C - \frac{d^2}{0.95p_d}$$

where W_C and L_C denote the cavity's physical width and length, respectively, whereas W_{eff} and L_{eff} represent the effective dimensions.

The full-mode SIW (FMSIW) is subsequently divided along the diagonal magnetic wall (AA') to obtain a HMSIW cavity, as illustrated in Fig. 2(b). The resulting HMSIW cavity maintains approximately the same fundamental resonant frequency as the original FMSIW structure. However, an open-ended magnetic boundary of the HMSIW cavity leads to electromagnetic energy leakage, as observed from the field distribution in Fig. 3(b). To suppress this unwanted field, we employ a row of shorting vias along the open magnetic boundary, as shown in Fig. 2(c). Furthermore, we introduce a long rectangular slot adjacent to the via-shielded boundary to form the effective magnetic wall of the HMSIW cavity.

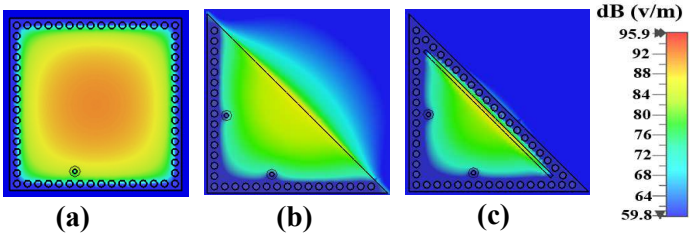


Fig. 3 E-field distribution: (a) FMSIW, (b) HMSIW, and (c) HMSIW with a shielded wall.

A rectangular slot divides the HMSIW cavity into two resonant sections of different dimensions, resulting in the Antenna-1 configuration illustrated in Fig. 2(d). Each cavity is independently fed through a 50 Ω coaxial feed. Under excitation at Ports 1 and 2, Cavities 1 and 2 exhibit resonances at 5.96 GHz and 7.68 GHz, respectively, with an inter-port isolation of −25 dB. To further improve isolation between the self-diplexing ports, we incorporate two additional slots in each cavity, positioned above and below the corresponding coaxial feed, as illustrated (Antenna-2) in Fig. 2(e). In the final configuration, three fluidic pockets are incorporated into each cavity by drilling through the ground plane and substrate to a depth of 1 mm. Here, air/DI water can be introduced as a fluidic dielectric medium to tune the operating frequency independently. After filling, the pockets are sealed with copper tape to restore and preserve ground-plane continuity.

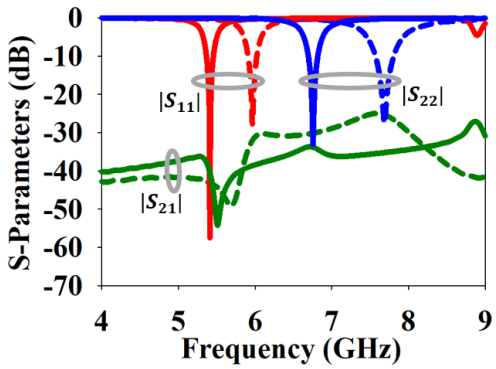


Fig. 4 Simulated S-parameters of Antenna I (dotted lines) and Antenna II (solid lines).

Fig. 4 compares the simulated S-parameter responses of self-diplexing antennas I and II. Antenna II exhibits resonances at 5.45 GHz and 6.75 GHz, with corresponding high inter-port isolation levels of −40 dB and −35 dB at the lower and higher frequencies, respectively. Compared with Antenna I, the additional slot configuration in Antenna II improves the isolation between the self-diplexing ports. Fig. 5 illustrates the corresponding electric-field distributions, confirming independent excitation of the two resonant cavities. After exciting port-1, the electric field is predominantly confined within cavity-1, resulting in resonance at 5.45 GHz. In contrast, after exiting port-2, the field concentrates within cavity-2, producing resonance at 6.75 GHz. These distributions confirm that the self-diplexing ports operate independently.

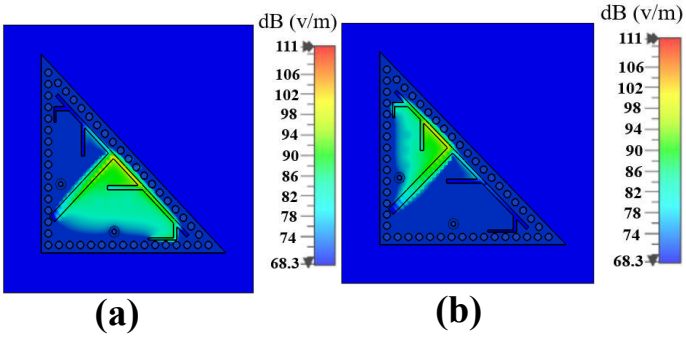


Fig. 5 Electric-field distributions: (a) Port 1 excited and (b) Port 2 excited.

3 FREQUENCY RECONFIGURATION

The main advantage of the proposed microfluidic self-diplexing antenna is its ability to independently tune its two resonant frequencies. To enable frequency reconfiguration, cylindrical microfluidic pockets are incorporated beneath each cavity and filled with deionized (DI) water, as illustrated in Fig. 2(f). The resonant frequencies of the two cavities can be tuned independently by selectively filling the DI water in these pockets.

The DI water has a dielectric constant of 78 with a loss tangent of 0.05 [33]. Its higher dielectric constant compared with air and the substrate material increases the effective permittivity of the cavity when DI water is introduced into the microfluidic pockets. This increase in effective permittivity reduces the resonant frequency. Conversely, filling fewer pockets with DI water decreases the effective permittivity, shifting the resonant frequency upward. Thus, varying the number of water-filled pockets in each cavity controls the resonant frequency. Table. 1 summarizes the resonant frequency variation and corresponding antenna characteristics, including simulated realized gain and total efficiency.

For cavity-1, when all fluidic pockets are air-filled, the antenna resonates at 5.45 GHz (Case 1). Conversely, filling the pockets completely with DI water shifts the resonance to 5.08 GHz, as observed in Case 4. By varying the number of DI-water-filled pockets in Cavity 1, the Port-1 resonant frequency can be continuously adjusted between 5.08 and 5.45 GHz across Cases 1–4. A similar tuning mechanism is employed for cavity-2. When all pockets contain air, the antenna resonates at 6.75 GHz in Case 4, whereas filling it completely with DI water reduces the resonant frequency to 6.37 GHz in Case 7. By varying the number of DI-water-filled pockets in Cavity 2, the Port-2 resonant frequency was tuned from 6.37 to 6.75 GHz for Cases 4–7. Fig. 6 present the simulated $|S_{11}|$ responses for the different fluid-filling conditions of cavity-1 and cavity-2, respectively.

Fig. 7 illustrates the simulated realized gain and total efficiency of the microfluidic self-diplexing antenna for different frequency-reconfiguration states. For Port-1, the resonant frequency is tuned to 5.08, 5.18, 5.29, and 5.45 GHz, while Port-2 is tuned

Table 1 Reconfiguration of frequency based on various fluid pocket filling

Case	No. of pockets filled with DI water		Frequency (GHz)		Gain (dBi)	
	Cavity-1	Cavity-2	f_1	f_2	f_1	f_2
1			**5.45**	6.75	5.60	5.65
2			**5.29**	6.75	5.56	5.65
3			**5.18**	6.75	5.47	5.65
4			**5.08**	**6.75**	5.45	5.65
5			5.45	**6.60**	5.60	5.61
6			5.45	**6.49**	5.60	5.59
7			5.45	**6.37**	5.60	5.60
8			5.08	6.37	5.45	5.60

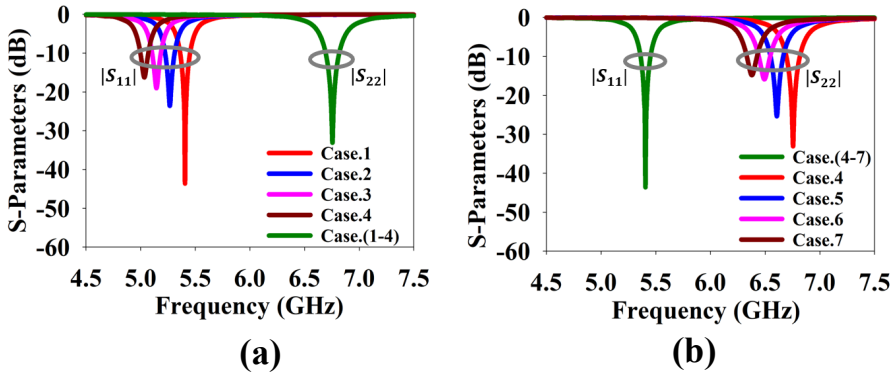


Fig. 6 Frequency shift with respect to $|S_{11}|$ for different filling cases in (a) cavity-1 and (b) cavity-2.

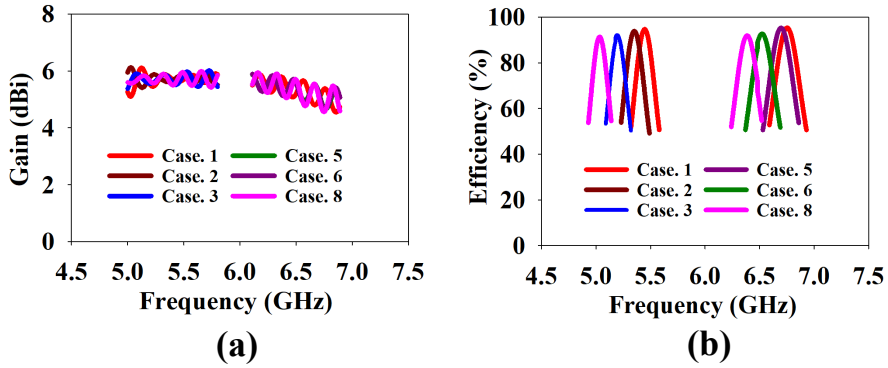


Fig. 7 Gain and efficiency for different DI-water filling cases listed in Table II

to 6.37, 6.49, 6.60, and 6.75 GHz for different fluid-loading cases. The realized gain remains above 5.45 dBi for all considered fluid-filling conditions, with a peak gain of 5.65 dBi. The antenna maintains efficiency above 90% for all DI water filling conditions, with a maximum total efficiency of 95%. The air-filled configurations exhibit higher efficiency than the DI water-loaded cases, likely because DI water has higher dielectric loss.

Aa shown in Fig. 8(a) the slot length L_{s1} increases from 10.4 to 11.6 mm, the resonant frequency shifts toward lower frequencies, accompanied by improved port isolation. Among the dimensions, $L_{s1} = 11.6$ mm provides the desired performance, yielding isolation levels exceeding 35 dB at both operating frequencies. Fig. 8(b) shows the simulated frequency responses obtained by varying the parameter L_{s2}. As L_{s2}

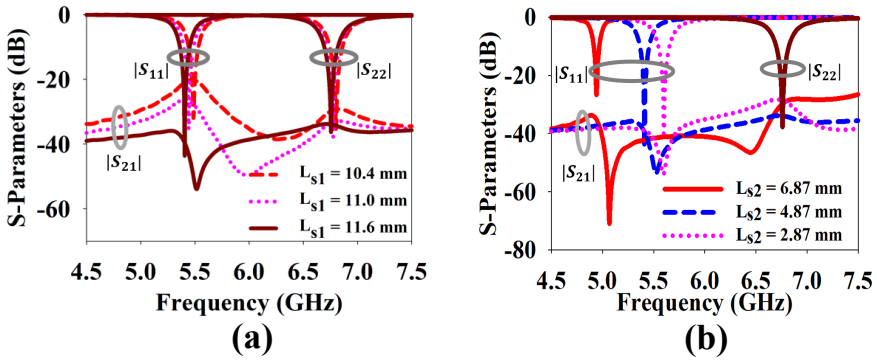


Fig. 8 Frequency response comparison for different values of (a) L_{s1} slot and (b) L_{s2} slot.

increases from 2.87 to 6.87 mm, the resonant frequency shifts downward. Based on the observed isolation characteristics, we consider $L_{s2} = 4.87$ mm the optimized value for the proposed antenna.

4 MIMO ANTENNA DESIGN

Fig. 9 illustrates the four-element, eight-port MIMO antenna system realized using microfluidic self-diplexing antenna elements. These elements are positioned in an orthogonal arrangement on a Rogers RT/duroid 5880 substrate to enable compact integration and improved spatial isolation.

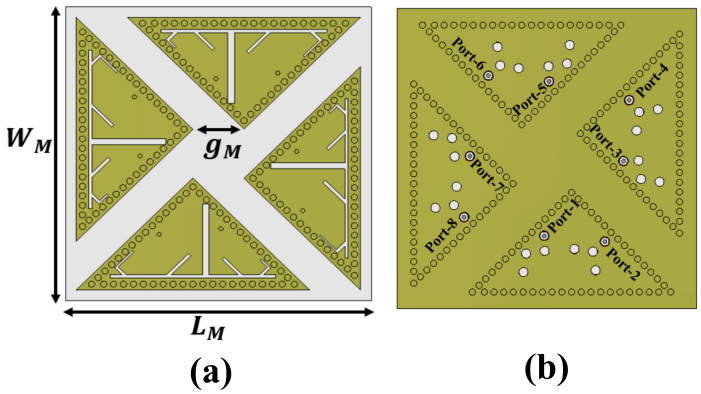


Fig. 9 MIMO antenna configuration for the proposed microfluidically reconfigurable self-diplexing antenna ($L_M = W_M = 48$ mm, $g_M = 8$ mm).

Fig. 10 illustrates the simulated S-parameter characteristics for the MIMO antenna system. The reflection coefficients (S_{ii}) match those of a single-element self-diplexing antenna, with port isolation (S_{ij}) greater than 22 dB. This indicates adequate isolation among the MIMO antenna elements.

In a MIMO antenna system, spatial diversity enables multiple antenna elements to transmit and receive information through distinct spatial channels, improving wireless communication reliability. To assess diversity performance and electromagnetic interaction among the antenna elements, we evaluate several MIMO performance parameters for the proposed configuration. The data is transmitted redundantly through spatial diversity. We compute several MIMO parameters to verify the spatial diversity of the MIMO antenna system.

The envelope correlation coefficient (ECC) is used to assess the correlation between the radiation characteristics of individual antenna elements in a MIMO system. An ECC value close to zero represents ideally uncorrelated antenna responses, whereas a value approaching unity indicates strong correlation. As shown in Fig. 11(a), the

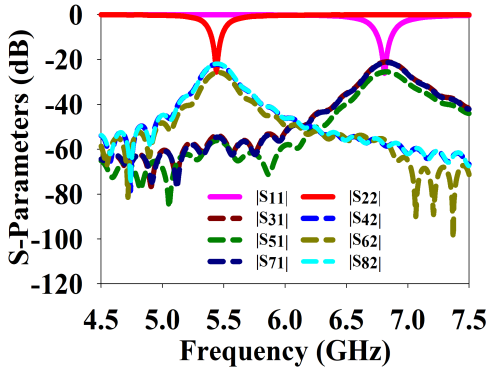


Fig. 10 Simulated reflection and transmission coefficients of the MIMO antenna system.

calculated ECC for the proposed antenna remains below 0.01 throughout the operating frequency range, demonstrating negligible correlation between antenna elements. The ECC is evaluated from the simulated S-parameters using (2) [34].

$$\mathrm{ECC} = \frac{\left|S_{ii}^{*}S_{ij} + S_{ji}^{*}S_{jj}\right|^{2}}{\left(1 - |S_{ii}|^{2} - |S_{ji}|^{2}\right)\left(1 - |S_{jj}|^{2} - |S_{ij}|^{2}\right)} \tag{2}$$

Here, S_{ii} and S_{jj} denote the reflection coefficients at ports (i) and (j), respectively, while S_{ij} and S_{ji} represent the transmission coefficients between these ports.

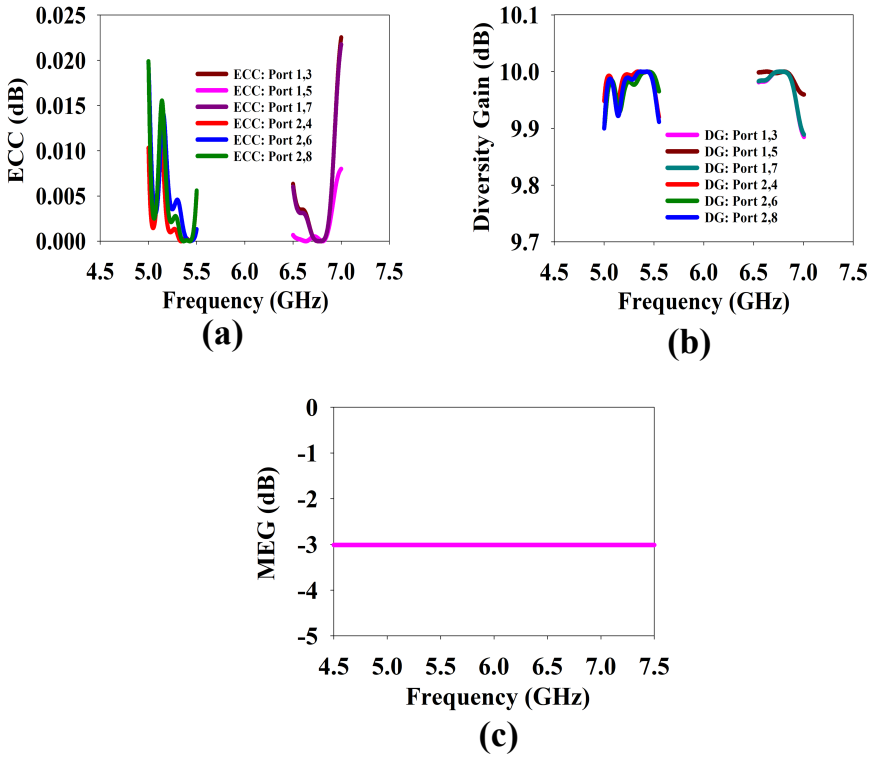


Fig. 11 Diversity performance metrics of MIMO antenna System: (a) ECC, (b) DG, and (c) MEG.

When the diversity mechanism is used, diversity gain (DG) indicates the improvement in link reliability achieved through diversity techniques. An ideal MIMO configuration exhibits a DG of 10 dB, corresponding to maximum diversity. For the proposed antenna, the DG is 9.9 dB across its operating frequency range, as shown

in Fig. 11(b), indicating effective spatial diversity. The ECC determines the diversity gain using (3).

$$DG = 10\sqrt{1 - 0.99\,ECC^2} \tag{3}$$

Another key metric for evaluating a MIMO antenna diversity under multipath propagation is the mean effective gain (MEG). It represents the average power of an antenna element relative to the incident power. For effective spatial diversity, the antenna elements should receive approximately equal average power. Accordingly, the ideal MEG is 0.5 on the linear scale, corresponding to −3 dB on the logarithmic scale. As presented in Fig. 11(c), the antenna system attains an MEG of −3.01 dB, indicating balanced power distribution among the antenna elements.

Channel capacity loss (CCL) is evaluated to assess how antenna coupling and correlation affect the information-carrying capability of the proposed MIMO system. Lower CCL values indicate better preservation of channel capacity. The CCL is determined using (4), with values less than 0.4 bits/s/Hz considered suitable for MIMO operation [34]. At the two operating frequencies, the proposed configuration maintains CCL values below 0.34 bits/s/Hz at 5.45 GHz and 0.15 bits/s/Hz at 6.75 GHz, confirming low channel-capacity degradation at both operating frequencies.

$$\mathrm{CCL} = -\log_2 \det\left(\psi^R\right) \quad ----------(4)$$

Here, ψ^R represents the receiver-side antenna correlation matrix, defined as follows:

$$\psi^R = \begin{pmatrix} \psi_{ii} & \psi_{ij} \\ \psi_{ji} & \psi_{jj} \end{pmatrix}$$

$$\psi_{ii} = 1 - \left(|S_{ii}|^2 + |S_{ij}|^2\right)$$
$$\psi_{ij} = -\left(S_{ii}^* S_{ij} + S_{ji}^* S_{jj}\right)$$
$$\psi_{ji} = -\left(S_{ji}^* S_{jj} + S_{ii}^* S_{ij}\right)$$
$$\psi_{jj} = 1 - \left(|S_{jj}|^2 + |S_{ji}|^2\right)$$

Table 2 Channel Capacity loss between various ports.

Ports	**CCL (bits/s/Hz)**	**Ports**	**CCL (bits/s/Hz)**
Port_14	0.3319	Port_23	0.1433
Port_15	0.3126	Port_26	0.1242
Port_18	0.3359	Port_27	0.1342

Fig. 12 compares the transmission coefficients for two MIMO configurations. When the antenna elements are intentionally displaced from the opposite configuration, isolation improves from 18 dB to 22 dB at lower frequencies.

5 RESULTS AND DISCUSSION

To experimentally verify the simulated performance, a prototype of the proposed antenna was fabricated using a Rogers RT/duroid 5880 substrate. Fig. 13 shows the fabricated antenna and experimental measurement setup. The fluid pockets are etched through the ground plane and substrate in each cavity to a depth of 1.00 mm. The antenna's performance was characterized inside an anechoic chamber using an MS46122B vector network analyzer (VNA).

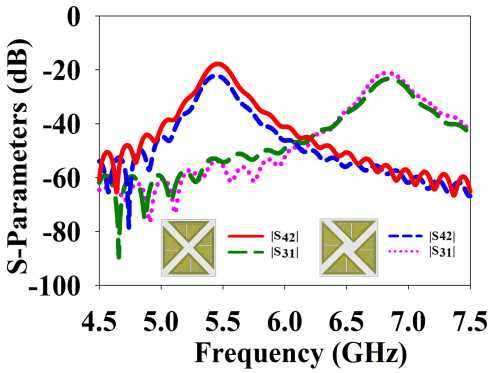
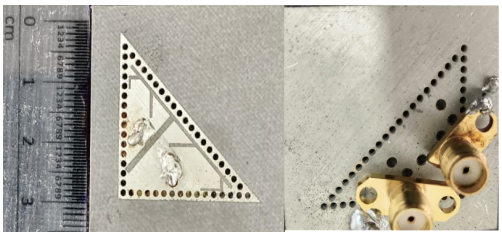
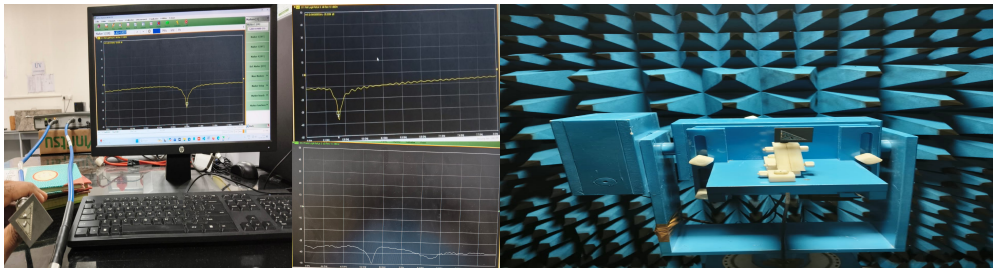


Fig. 12 Transmission coefficients for different MIMO configurations.



(a)



(b)

Fig. 13 Fabricated self-diplexing antenna prototype: (a) top and bottom views; (b) experimental measurement arrangement.

Fig. 14 illustrates the simulated and measured S-parameter responses of the antenna with air-filled pockets. The measured reflection coefficients indicate resonances at 5.48 GHz for Port 1 and 6.83 GHz for Port 2, while the port isolation exceeds 35 dB. The S-parameter responses for different deionized water filling conditions are shown in Fig. 15. As shown in Fig. 15(a), the measured resonant frequency of cavity-1 can be tuned across 5.10 GHz-5.48 GHz under different DI water-filling conditions. Similarly, Fig. 15(b) shows that the frequency bands shift from 6.30 GHz to 6.83 GHz across different DI water-filling cases in cavity-2.

Fig. 16(a) shows the fabricated MIMO antenna prototype implemented on a 48 mm × 48 mm × 1.57 mm Rogers RT/5880 substrate. The four radiating elements are arranged orthogonally to provide the desired isolation characteristics while maintaining a compact size. The prototype is experimentally tested to verify the simulated MIMO performance. As illustrates in Fig. 16(b), the measured S-parameter responses closely match the simulated responses. The measured inter-element isolation exceeds 20 dB, confirming effective mutual coupling reduction. The strong agreement between the simulated and experimental responses verifies the practical feasibility of the proposed antenna design.

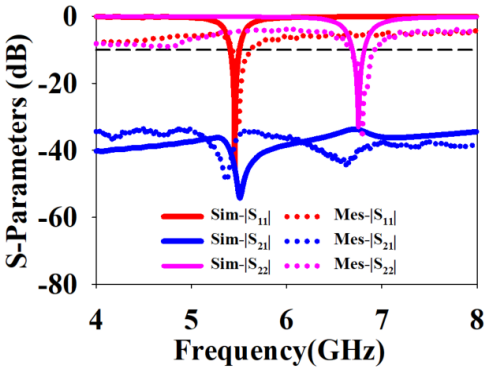


Fig. 14 Simulated and experimental S-Parameter characteristics of Self-Diplexing Antenna.

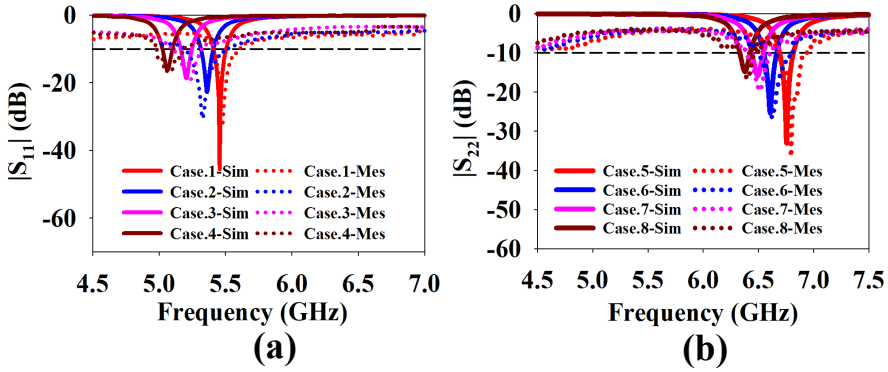


Fig. 15 Reflection coefficient for different DI water-filling cases: (a) cavity-1, (b) cavity-2.

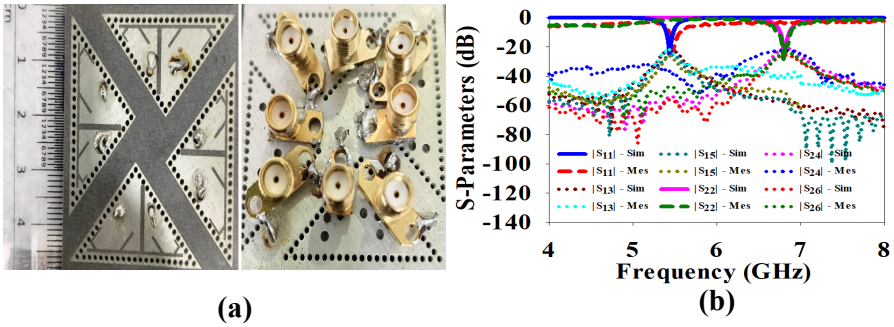


Fig. 16 MIMO antenna: (a) Fabricated prototype; (b) simulated and measured S-parameters.

The simulated and experimental radiation characteristics of the self-diplexing antenna, considering the $\phi = 0°$ and $\phi = 90°$ cut planes, are shown in Fig. 17. The results demonstrate that the antenna exhibits predominantly broadside radiation characteristics in both principal planes. A good correspondence is observed between simulated and experimental patterns, with minor discrepancies due to measurement uncertainty. The co-polarized radiation components remain dominant over cross-polarized components in both principal planes. Fig. 18 presents the simulated and measured radiation characteristics of the proposed antenna with DI water loading. The radiation patterns remain nearly consistent after DI-water loading, confirming that the microfluidic tuning approach provides frequency reconfiguration without significantly degrading the radiation behavior.

Table. 3 compares the proposed antenna with previously reported self-diplexing antennas. The proposed design provides high port isolation and gain across both

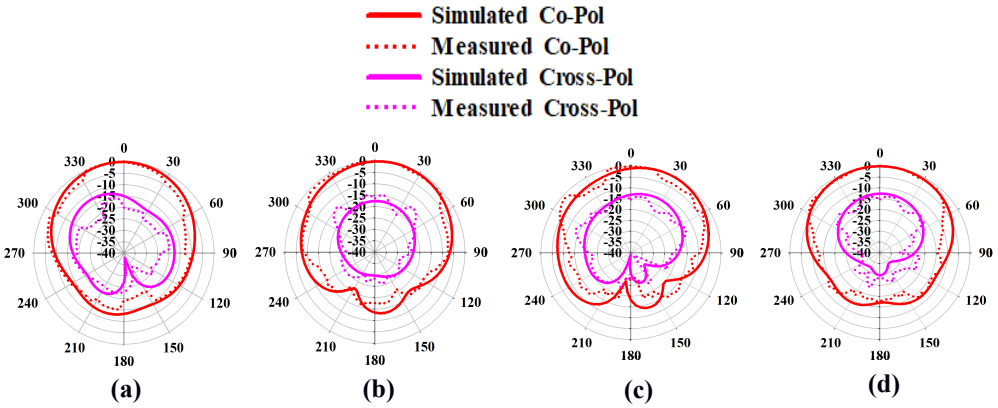


Fig. 17 2D radiation patterns without DI water loading: (a) $\phi = 0°$, 5.45 GHz; (b) $\phi = 90°$, 5.45 GHz; (c) $\phi = 0°$, 6.75 GHz; (d) $\phi = 90°$, 6.75 GHz.

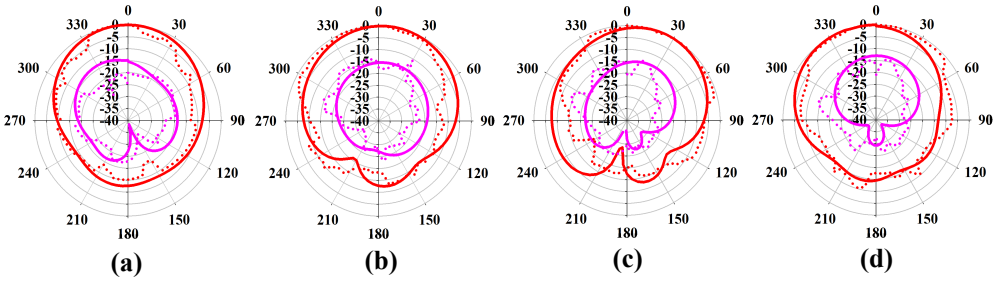


Fig. 18 2D radiation patterns with DI water loading: (a) $\phi = 0°$, 5.08 GHz; (b) $\phi = 90°$, 5.08 GHz; (c) $\phi = 0°$, 6.36 GHz; (d) $\phi = 90°$, 6.36 GHz.

Table 3 Comparative analysis of the proposed self-diplexing antenna with previously reported designs.

Ref	Frequency (GHz)	Isolation (dB)	Gain (dB)	Size (λ_g^2)	Efficiency (%)	Reconfigurability	MIMO
[9]	8.26/10.46	27.9	4.3/4.2	0.37	—	No	—
[10]	9.5/10.5	29	5.75/5.95	0.43	—	No	—
[12]	9.00/11.2	25	4.3/4.2	0.38	—	No	—
[15]	6.44/7.09	30	3.1/4.8	0.30	—	No	—
[20]	3.395/5.75	—	0.6/2.2	0.27	68	Varactor Diode	—
[21]	3.9-4.37 4.63-5.34	22	0.8-3.82 0.98-4.48	0.61	64	Varactor Diode	—
[22]	2.64-2.82 3.15-3.41	20	4.9-5.6 4.6-5.5	0.85	60	Varactor Diode	—
[23]	3.77-4.59 4.96-6.10	21	4.85-5.87 4.96-6.50	0.28	—	Varactor Diode	—
[29]	2.7-3.47 4.05-4.96	20.35	1.97-4.43 3.66-4.95	0.31	70-90	Liquid Dielectric	—
[30]	3.25-3.52 4.5-5.04	30.3	3.34-3.93 2.69-3.43	0.34	—	Liquid Dielectric	—
[31]	3.26-3.75 5.07-5.90	31	3.85-4.14 5.03-5.45	0.078	—	Liquid Dielectric	—
[32]	3.5-3.8 5.53-6.2	27	5.04-5.58 5.26-5.96	0.22	88-95	Liquid Dielectric	—
This	**5.08-5.45 6.36-6.75**	**35**	**5.45-5.60 5.60-5.65**	**0.23**	**90-95**	**Liquid Dielectric**	**Yes**

operating bands, with a high total efficiency of 90–95%, and uses liquid-dielectric-based frequency reconfiguration without active switching devices. Unlike the reported self-diplexing antennas, which are restricted to single-element designs, the proposed antenna integrates microfluidic reconfiguration into a MIMO system.

6 Conclusion

This work presents a microfluidically reconfigurable self-diplexing MIMO antenna based on a half-mode SIW technology for Wi-Fi 6/6E applications. A diagonally shielded magnetic wall suppresses electromagnetic leakage, while a rectangular slot divides the cavity into two unequal resonant cavities, enabling self-diplexing at 5.45 and 6.75 GHz with inter-port isolation greater than 35 dB. Frequency reconfiguration is realized using three microfluidic pockets inserted in each cavity, selectively loaded with deionized water. The measured operating frequency bands are from 5.10–5.48 GHz and 6.30–6.83 GHz, respectively. Furthermore, a four-element, eight-port MIMO configuration is developed, and the element positions are optimized, achieving measured inter-element isolation below -20 dB over the intended bands. The evaluated MIMO metrics remain within acceptable limits. The proposed design integrates self-diplexing, liquid-dielectric frequency reconfiguration, and MIMO functionality within a compact SIW structure while maintaining acceptable gain and efficiency in the operating bands, making it suitable for wireless communication systems.

Data Availability

The datasets used and/or analyzed during the current study are available from the corresponding author upon reasonable request.

References

[1] Hu, W., Yin, Y.-Z., Fei, P., Yang, X.: Compact triband square-slot antenna with symmetrical l-strips for wlan/wimax applications. IEEE Antennas and Wireless Propagation Letters **10**, 462–465 (2011) https://doi.org/10.1109/LAWP.2011.2154372

[2] Liu, H., Jiang, H., Guan, X., Lei, J., Li, S.: Single-feed slotted bowtie antenna for triband applications. IEEE antennas and wireless propagation letters **12**, 1658–1661 (2013)

[3] Chen, H., Yang, X., Yin, Y., Fan, S., Wu, J.: Triband planar monopole antenna with compact radiator for wlan/wimax applications. IEEE Antennas and Wireless Propagation Letters **12**, 1440–1443 (2013)

[4] Su, S.-W., Lee, C.-T., Chen, S.-C.: Very-low-profile, triband, two-antenna system for wlan notebook computers. IEEE Antennas and Wireless Propagation Letters **17**(9), 1626–1629 (2018)

[5] Tan, Q., Chen, F.-C.: Triband circularly polarized antenna using a single patch. IEEE Antennas and Wireless Propagation Letters **19**(12), 2013–2017 (2020)

[6] Montero-de-Paz, J., Ugarte-Munoz, E., Herraiz-Martinez, F.J., Gonzalez-Posadas, V., Garcia-Munoz, L.E., Segovia-Vargas, D.: Multifrequency self-diplexed single patch antennas loaded with split ring resonators. Progress In Electromagnetics Research **113**, 47–66 (2011) https://doi.org/10.2528/PIER10121703

[7] Boyle, K.R., Udink, M., Graauw, A., Ligthart, L.P.: A dual-fed, self-diplexing pifa and rf front-end. IEEE Transactions on Antennas and Propagation **55**(2),

373–382 (2007) https://doi.org/10.1109/TAP.2006.889852

[8] Lu, Y.-C., Lin, Y.-C.: A mode-based design method for dual-band and self-diplexing antennas using double t-stubs loaded aperture. IEEE Transactions on Antennas and Propagation **60**(12), 5596–5603 (2012) https://doi.org/10.1109/TAP.2012.2211852

[9] Nandi, S., Mohan, A.: An siw cavity-backed self-diplexing antenna. IEEE Antennas and Wireless Propagation Letters **16**, 2708–2711 (2017) https://doi.org/10.1109/LAWP.2017.2743017

[10] Khan, A.A., Mandal, M.K.: Compact self-diplexing antenna using dual-mode siw square cavity. IEEE Antennas and Wireless Propagation Letters **18**(2), 343–347 (2019) https://doi.org/10.1109/LAWP.2018.2890790

[11] Barik, R.K., Cheng, Q.S., Dash, S.K.K., Pradhan, N.C., Karthikeyan, S.S.: Compact high-isolation self-diplexing antenna based on siw for c-band applications. Journal of Electromagnetic Waves and Applications **34**(7), 960–974 (2020) https://doi.org/10.1080/09205071.2020.1763859 https://doi.org/10.1080/09205071.2020.1763859

[12] Mukherjee, S., Biswas, A.: Design of self-diplexing substrate integrated waveguide cavity-backed slot antenna. IEEE Antennas and Wireless Propagation Letters **15**, 1775–1778 (2016) https://doi.org/10.1109/LAWP.2016.2535169

[13] Priya, S., Dwari, S.: A compact self-triplexing antenna using hmsiw cavity. IEEE Antennas and Wireless Propagation Letters **19**(5), 861–865 (2020) https://doi.org/10.1109/LAWP.2020.2982533

[14] Iqbal, A., Mabrouk, I.B., Al-Hasan, M., Nedil, M., Denidni, T.A.: Wideband substrate integrated waveguide antenna for full-duplex systems. IEEE Antennas and Wireless Propagation Letters **21**(1), 212–216 (2022) https://doi.org/10.1109/LAWP.2021.3125610

[15] Kumar, A., Chaturvedi, D., Raghavan, S.: Design of a self-diplexing antenna using siw technique with high isolation. AEU - International Journal of Electronics and Communications **94**, 386–391 (2018) https://doi.org/10.1016/j.aeue.2018.07.031

[16] Tong, Y., Qian, Z., Cao, W., Shi, S., Cai, Y.: Design of frequency duplex and triplex antennas based on quarter-mode substrate integrated waveguide. IET Microwaves, Antennas & Propagation **13**(4), 414–419 (2018) https://doi.org/10.1049/iet-map.2018.5080 https://ietresearch.onlinelibrary.wiley.com/doi/pdf/10.1049/iet-map.2018.5080

[17] Jin, C., Li, R., Alphones, A., Bao, X.: Quarter-mode substrate integrated waveguide and its application to antennas design. IEEE Transactions on Antennas and Propagation **61**(6), 2921–2928 (2013) https://doi.org/10.1109/TAP.2013.2250238

[18] Kumari, P., Das, S.: A mimo antenna system using self-decoupled emsiw dual-beam antenna elements. IEEE Access **10**, 1339–1345 (2022) https://doi.org/10.1109/ACCESS.2021.3139269

[19] Lai, Q., Fumeaux, C., Hong, W., Vahldieck, R.: Characterization of the propagation properties of the half-mode substrate integrated waveguide. IEEE Transactions on Microwave Theory and Techniques **57**(8), 1996–2004 (2009) https://doi.org/10.1109/TMTT.2009.2025429

[20] Boukarkar, A., Lin, X.Q., Jiang, Y.: A dual-band frequency-tunable magnetic dipole antenna for wimax/wlan applications. IEEE Antennas and Wireless Propagation Letters **15**, 492–495 (2016) https://doi.org/10.1109/LAWP.2015.2454001

[21] Boukarkar, A., Lin, X.Q., Jiang, Y., Yu, Y.Q.: A tunable dual-fed self-diplexing patch antenna. IEEE Transactions on Antennas and Propagation **65**(6), 2874–2879 (2017) https://doi.org/10.1109/TAP.2017.2689035

[22] Iqbal, A., Tiang, J.J., Lee, C.K., Mallat, N.K.: Siw cavity backed self-diplexing tunable antenna. IEEE Transactions on Antennas and Propagation **69**(8), 5021–5025 (2021) https://doi.org/10.1109/TAP.2021.3060024

[23] Wang, G., Polley, T., Hunt, A., Papapolymerou, J.: A high performance tunable rf mems switch using barium strontium titanate (bst) dielectrics for reconfigurable antennas and phased arrays. IEEE Antennas and Wireless Propagation Letters **4**, 217–220 (2005) https://doi.org/10.1109/LAWP.2005.851065

[24] Erdil, E., Topalli, K., Unlu, M., Civi, O.A., Akin, T.: Frequency tunable microstrip patch antenna using rf mems technology. IEEE Transactions on Antennas and Propagation **55**(4), 1193–1196 (2007) https://doi.org/10.1109/TAP.2007.893426

[25] Van Caekenberghe, K., Sarabandi, K.: A 2-bit ka-band rf mems frequency tunable slot antenna. IEEE Antennas and Wireless Propagation Letters **7**, 179–182 (2008) https://doi.org/10.1109/LAWP.2008.921390

[26] Shamim, A., Bray, J.R., Hojjat, N., Roy, L.: Ferrite ltcc-based antennas for tunable sop applications. IEEE Transactions on Components, Packaging and Manufacturing Technology **1**(7), 999–1006 (2011) https://doi.org/10.1109/TCPMT.2011.2143411

[27] Liang, J., Yang, H.Y.D.: Microstrip patch antennas on tunable electromagnetic band-gap substrates. IEEE Transactions on Antennas and Propagation **57**(6), 1612–1617 (2009) https://doi.org/10.1109/TAP.2009.2019928

[28] Reddy, M.G., Subramanian, K.S., Pradhan, N.C., Koziel, S.: Frequency-reconfigurable hybrid siw-based self-diplexing antenna using solid and liquid dielectric loading. IEEE Transactions on Circuits and Systems II: Express Briefs **71**(5), 2624–2628 (2024) https://doi.org/10.1109/TCSII.2023.3347437

[29] Reddy, M.G., Pradhan, N.C., Karthikeyan, S.S.: Investigation on tuning capabilities of self-diplexing antenna using different liquid dielectrics. Journal of Electromagnetic Waves and Applications **37**(10-12), 1011–1022 (2023) https://doi.org/10.1080/09205071.2023.2220091

[30] Pradhan, N.C., Reddy, M.G., Subramanian, K.S., Barik, R.K., Koziel, S., Cheng, Q.S.: Microfluidic siw-based tunable self-diplexing antenna for sub-6 ghz band applications. IEEE Transactions on Circuits and Systems II: Express Briefs **70**(4), 1435–1439 (2023) https://doi.org/10.1109/TCSII.2022.3224234

[31] Kim, J., Shin, H., Wi, S., *et al.*: 2 x 2 mimo dual-wideband ground radiation antenna with a t-shaped isolator for wi-fi 6/6e/7 applications. Scientific Reports **15**, 85 (2025) https://doi.org/10.1038/s41598-024-84782-

[32] Dkiouak, A., Rahmani, F., El Ouahabi, M., Zakriti, A., Baghouri, M., El Mamouni, A.: A dual-port mimo antenna system for 5g and wi-fi 6e communications using a parasitic element. e-Prime - Advances in Electrical Engineering,

Electronics and Energy **10**, 100850 (2024) https://doi.org/10.1016/j.prime.2024.100850

[33] Huang, Y., Xing, L., Song, C., Wang, S., Elhouni, F.: Liquid antennas: Past, present and future. IEEE Open Journal of Antennas and Propagation **2**, 473–487 (2021) https://doi.org/10.1109/OJAP.2021.3069325

[34] Chaturvedi, D., Jadhav, P., Althuwayb, A.A., Aliqab, K.: A compact 2-port qmsiw cavity-backed mimo antenna with varied frequencies using csrr-slot angles for wban application. IEEE Access **12**, 100506–100514 (2024) https://doi.org/10.1109/ACCESS.2024.3425520

Author Contributions.

G. Krishna Reddy: conceived the study, designed the antenna, performed the electromagnetic simulations, fabricated and experimentally characterized the prototypes, analyzed the results, and prepared the original manuscript. Goutam Rana and Jyotibhusan Padhi: supervised the research, helped interpret the results, and critically reviewed and revised the manuscript. All authors reviewed and approved the final manuscript.

Funding.

The authors declare that no funding was received for this research.